CrystEngComm

Accepted Manuscript

This article can be cited before page numbers have been issued, to do this please use: A. Kubarev and M. B. Roeffaers, *CrystEngComm*, 2017, DOI: 10.1039/C7CE00074J.

View Article Online
DOI: 10.1039/C7CE00074J

CrystEngComm

COMMUNICATION

Surface acid-base catalytic activity of ZIF-8 revealed by super-resolution fluorescence microscopy

Received 00th January 20xx,
Accepted 00th January 20xx

DOI: 10.1039/x0xx00000x

www.rsc.org/

A. V. Kubarev and M. B. J. Roeffaers*

We investigated the catalytic activity of ZIF-8 in the fluorescein diacetate hydrolysis via super-resolution fluorescence microscopy. Acid-base activity is detected only on the outer surface and crystalline defects. Oleic acid etching introduces extra porosity and allows for catalytic conversions inside of the crystals, but leads to overall activity loss.

In recent years, metal-organic frameworks (MOFs) have been studied extensively as heterogeneous catalysts.[1–3] One of the main advantages of MOFs over the more traditional inorganic porous materials is the chemical variability offered by the hybrid framework. Numerous MOF frameworks have been described by varying metal cation as well as organic linkers. As both can be varied independently this offers unique opportunities for the development of bi-functional catalysts. One industrial process which could benefit from improved bifunctional acid-base catalysts is the synthesis of biodiesel. In this process fatty acid methyl esters are obtained from a transesterification of triglycerides. Traditionally (mixed) metal oxides and hydroxides have been extensively investigated for this purpose. The complex nature in surface sites and the limited amount of control over them have triggered research to investigate alternative materials. Several MOFs for example have been shown to be active in transesterification reactions.[4,5] In particular, one exceptionally stable[6] MOF type, zeolite imidazolate framework ZIF-8, is active in the (trans)esterification reactions,[7,8] as well is in the range of other acid-base catalysed reactions.[9–12] However, it is not straightforward to identify the catalytic active sites from the crystal structure of ZIF-8. Theoretically, the structure of ZIF-8 does not possess low-coordinated zinc atoms that could act as a Lewis acid, neither its imidazolate linkers bear an accessible nitrogen that could act as base. Therefore, the intrinsic catalytic activity of non-functionalized ZIF-8 posed a question about the type and location of its active sites. Several investigations of ZIF-8 catalytic properties have been conducted. In particular, Chizallet et al showed that ZIF-8 can dissociate alcohols what is necessary for transesterification, and suggested that coordinatively undersaturated Zn(II) species as acid sites are located with N-moieties and OH groups as basic sites at the external surface of ZIF-8 or at crystal defects.[7] However, all prior investigations have been done at the macro scale with bulk characterization techniques such as catalytic testing and infrared spectroscopy. For example, the conclusions about the active sites location are made based on indirect observations, such as shifts in frequency of carbon monoxide absorbed at ZIF-8. The observed CO-vibration frequencies were attributed to CO adsorbed on sites at the outer surface of the crystal based on supporting DFT-calculation. These techniques do not have the spatial resolution to directly probe the location of catalytic reactions or to pinpoint active sites in the individual catalyst crystals. In our view the appropriate approach to locate the active sites lies in the use of microscopy techniques. In particular, fluorescence microscopy has been shown to be a suitable tool for investigating of the single-crystal catalytic activity of a wide variety of heterogeneous catalysts, such as zeolites,[13–18] fluid catalytic cracking catalysts,[19] layered double hydroxides,[20] metal nanoparticles[21,22] and MOFs.[23] In this approach the catalytically active zones are selectively stained by the formation of fluorescent reaction products. Nanoscale reactivity maps, with resolutions below the optical diffraction limited resolution of a few hundreds of nanometeres, are based on the localization of individual catalytic conversions of fluorogenic – non fluorescent – reactants into strongly fluorescent products. This single molecule localization-based variant of fluorescence microscopy specifically designed for catalysis research is called Nanometre Accuracy by Stochastic Chemical reActions (NASCA) microscopy.[24] NASCA microscopy allows for detection of individual catalytic turnovers with a lateral resolution of tens of nm. Therefore, in this work NASCA microscopy was selected as technique of choice for the precise localization of the catalytic activity displayed by individual ZIF-8 crystals.

Center for Surface Chemistry and Catalysis, KU Leuven, Celestijnenlaan 200F, postbox 2461, 3001 Leuven, Belgium
E-mail: maarten.roeffaers@kuleuven.be
Electronic Supplementary Information (ESI) available: Full description of experimental methods, Supplementary figures S1,S2.
See DOI: 10.1039/x0xx00000x

For our investigation we synthesized ZIF-8 materials according to the procedure described by Bux et al.[25] This method allowed us to obtain a powdered sample that largely consists of well-defined crystals of truncated rhombic dodecahedron morphology with a wide size distribution – approximate crystal dimensions range from 5 to 25 µm. Crystals with these dimensions are perfectly suited for NASCA microscopy, which would also work with smaller crystals; the limited axial resolution of about 500 nm, related to the optical section that is sharply in focus,[26] simplifies interpretation. The use of larger crystals has an additional practical advantage as optical transmission microscopy, which is diffraction limited in resolution, was used to select and identify the crystals under study in the catalytic experiment.

As the use of fluorescence microscopy and by extension NASCA microscopy requires strongly fluorescent reaction products to pinpoint the location of catalytic activity it is not possible to directly observe the transesterification of triglycerides. Instead, we used in this work fluorescein diacetate (FDA) hydrolysis as an appropriate model reaction (**Figure 1**); the catalytic hydrolysis leads to the formation of individual fluorescein molecules (**Figure 2B, inset**). Such single catalytic events can be captured by the EM-CCD camera, using the correct colour filters, and these catalytic events are consecutively localized with nanometre precision to uncover the distribution of catalytic conversions throughout the ZIF-8 crystal.[17,20,24] This reaction is not only mechanistically similar to transesterification of triglycerides, the molecular size of FDA (minimal projection diameter = 12.08 Å) is comparable to size of triglycerides (minimal projection diameter for oleic acid triglyceride = 17.60 Å) and similar to triglycerides FDA is larger than ZIF-8 aperture size of 3.4 Å.[6]

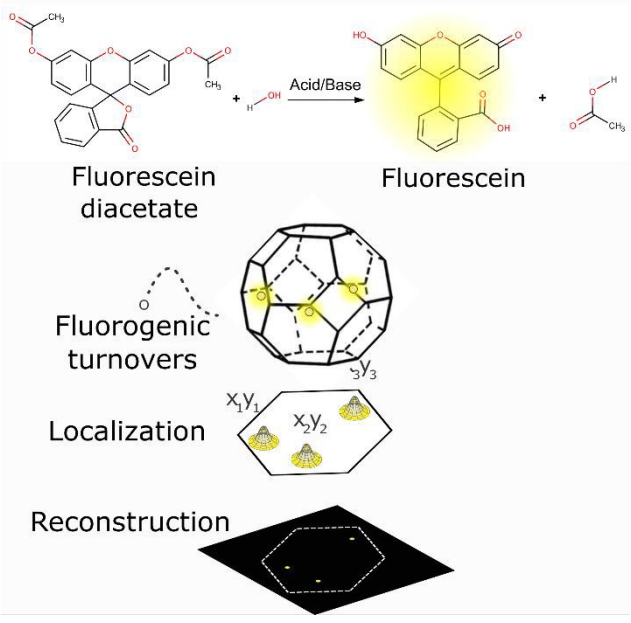

Figure 1. Schematic representation of the NASCA microscopy approach.

Figure 2 shows an example of the NASCA aproach using FDA as probe molecule revealing the location of catalytic activity on an individual ZIF-8 crystal. The optical transmission image (Figure 2A) gives a clear view on the truncated rhombic dodecahedron shaped ZIF-8 crystal with a very clear defect at the right side of the crystal. As transmission image is the result of absorption and scattering events along the optical pathlength it does not provide precise information on the stuctural features and it for sure does not yield insight into the location of catalytically active centres. After FDA addition, the locations of catalytic activity light up in the wide-field fluorescence microscope (Figure 2B) as individual bright emitters (Figure 2B, inset). The full NASCA experiment consists of recording 1000-10000 consecutive frames of 50 ms integration time each. The FDA molecules are stochastically converted at the catalytic active sites resulting in bright fluorescein molecules that only appear briefly (~100 ms on average or 2 consecutive frames) as the product is photobleached or diffuses away. The positions of each catalytic turnover, localized in each frame and corrected for reappearing molecules, were plotted as scatter plot (Figure 2C) or as accumulated reactivity map in which all conversions inside a 50x50x800 nm^3 voxels are counted (Figure 2D). In contrast to optical transmission imaging, only single fluorescent products formed in a thin optical slice are recorded and localized effectively. Optical slicing allows to map the reactivity of individual particles in 3D.

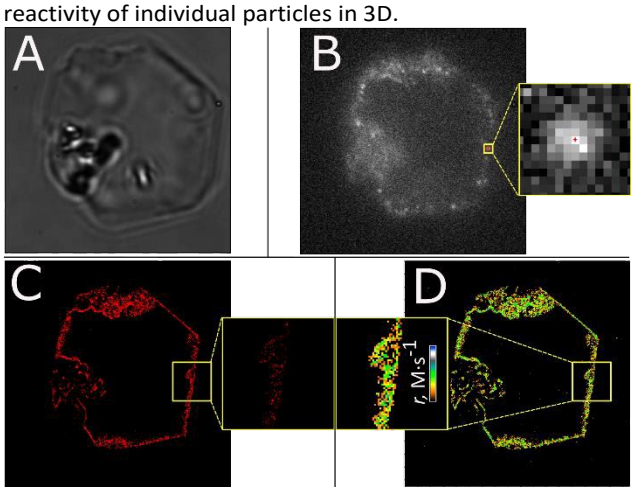

Figure 2. Procedure for NASCA microscopy approach as exemplified by ZIF-8 catalysis of FDA hydrolysis. A – bright-field transmission image, B – single frame of wide-field fluorescence microscopy-acquired movie, B inset – example of a localised single emitter, C – scatter plot of all localized position for the acquired movie, C inset – magnification of the area of interest, D – NASCA reactivity map of the catalytic activity reconstructed for 50x50x800 nm^3 voxels (xyz) for the duration of ≈ 150 s, D inset – magnification of the area of interest, false colour shows the observed reaction rate in logarithmic scale from $2.2 \cdot 10^{-9}$ to $6 \cdot 10^{-7}$ M·s^{-1}.

The catalytic activity distribution of a single ZIF-8 crystal is presented in **Figure 3** as a set of optical slices along the depth of the crystal. These NASCA images obtained for the different

optical slices spaced ~2 µm apart were recorded from the bottom to the top of the crystal and are presented with the identical colour scale. Clearly, the catalytic activity is restricted to the outer surface of the crystal. This observed surface-limited activity is in agreement with suggestion of Chizallet et al.[7,27] Even more so, several other studies have indicated that active sites of many MOFs are most likely linked to defects in the crystalline structure.[28,29] Correspondingly, in some optical slices the activity at crystal defect is captured showing catalytic conversions also at the internal parts of the ZIF-8 crystal (Figure 3B-E). Some facets of the crystal are almost free of defects at every depth, while others are rich with defects. Such uneven defect distribution occurs stochastically only in some of ZIF-8 crystals, as additional observations showed (**Figure S1**).

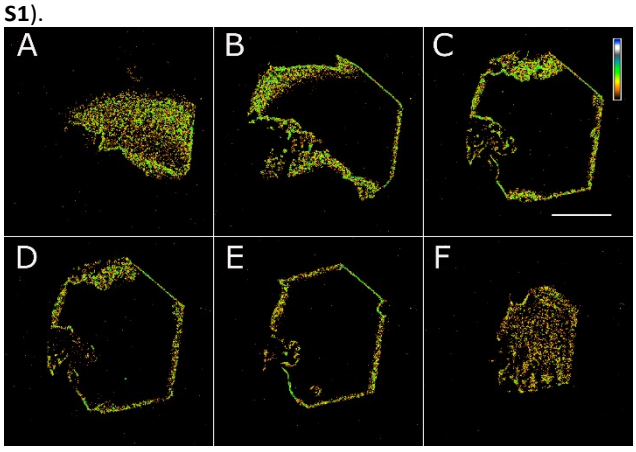

Figure 3. NASCA reactivity maps of FDA hydrolysis catalysed inside of a ZIF-8 crystal. A – bottom surface of the crystal, B-E – gradually progressive slices in the bulk of the crystal, F – top surface of the crystal. Scale bar is 5 µm; maps are reconstructed for 50x50x800 nm^3 voxels (xyz) for the duration of ≈ 150 s; false colour shows the observed reaction rate in logarithmic scale from $2.2 \cdot 10^{-9}$ to $6 \cdot 10^{-7}$ $M \cdot s^{-1}$.

Therefore we hypothesised that the catalytic activity of ZIF-8 can be improved via introduction of extraframework pores hence increasing the effective surface area. Wee et al. described spontaneous formation of mesopores in ZIF-8 during the direct glycerol esterification with oleic acid.[8] They proposed that oleic acid treatment alone can be a viable procedure for mesopore introduction. We applied the suggested oleic acid treatment to ZIF-8, which resulted in crystals etching (**Figure 4A,B**). It is clear that the catalytic activity of etched ZIF-8 is not exclusively restricted to the outer surface (Figure 4C-E), in line with our expectations. While the majority of reaction events still take place at the outer surface, some FDA molecules are able to reach inner regions of the crystals; prolonged etching in the oleic acid solution led to complete fragmentation of the ZIF-8 crystals. Surprisingly, the overall catalytic activity of ZIF-8 seems to have decreased as a result of oleic acid etching as can be seen in smaller reaction rate values detected in etched ZIF-8 crystals. The oleic acid treatment however leads to a significant rise in background fluorescence, complicating a precise quantitative comparison between catalytic activities based on the NASCA experiment.

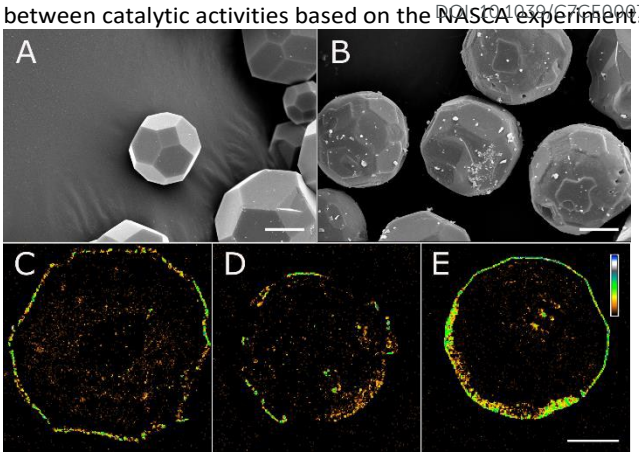

Figure 4. Effect of oleic acid etching on structure and activity of ZIF-8 crystals. A-B – SEM micrographs of original (A) and etched(B) ZIF-8 crystals, scale bars are 10 µm; C-E – NASCA reactivity maps of FDA hydrolysis catalysed inside of three exemplary etched ZIF-8 crystals. Scale bar is 5 µm, maps are reconstructed for 100x100x800 nm^3 voxels (xyz) for the duration of ≈ 500 s; false colour shows the observed reaction rate in logarithmic scale from $2.9 \cdot 10^{-10}$ to $2.6 \cdot 10^{-7}$ $M \cdot s^{-1}$.

The observations from the NASCA experiment were cross-checked and validated by determining the catalytic behaviour at the bulk scale with 0.5 mg of ZIF-8 powder and using FDA concentration of 5 uM in 3 ml of water. Due to the fluorogenic nature of this reaction, the bulk catalytic activity can easily be monitored using a standard spectrophotometer or fluorimeter. In this experiment the fluorescein product concentration was measured using the optical adsorption at 491 nm wavelength after 24 hours. The bulk-scale catalytic activity of the etched ZIF-8 based on the measured fluorescein concentration was estimated to be about 80% of the activity of the original catalyst sample. It is important to note that in the study of Wee et al.[8] etched sample activity could not be compared with original sample due to oleic acid etching being the inherent side reaction. To the best of our knowledge no other investigation was studying the effect of oleic acid on structure and activity of ZIF-8. Our results for the first time show that in addition to the increase in surface area, oleic acid etching is reducing the number or accessibility of active sites. Such a reduction in activity is probably related to the poisoning of base active sites by oleic acid preventing FDA molecules from activation. Our attempts to remove oleic acid from the sample by washing it with 1-heptanol, heptane, methanol solution of 2-methylimidazol, and methanol did not improve catalytic performance (**Figure S2**). We conclude that the poisoning of the oleic acid is rather strong and that removal is not trivial.

In conclusion, we investigated the catalytic activity of ZIF-8 in FDA hydrolysis reaction as a reference for its activity as solid catalyst e.g. in the triglycerides transesterification. The sites of activity of the microporous ZIF-8 are limited to the outer crystal surface and surface of the bulk defects, providing a direct proof to the earlier

proposed hypothesis. Introducing additional extraframework porosity by the oleic acid etching allows for catalysis deeper inside the crystal, however at a lower reaction rate due to poisoning of the active sites. Further research on the optimizing catalytic performance of the modified ZIF-8 catalysts in transesterification reactions could focus on finding a procedure to effectively remove the porosity inducing agent (oleic acid) or alternative porosity inducing agents that can be removed more easily.

Acknowledgements

The authors thank Peter Dedecker for assistance with super-resolution localization analysis routine.[30] The authors thank the "Fonds voor Wetenschappelijk Onderzoek" (Grants G0962.13 and G.0B39.15), the KU Leuven Research Fund (C14/15/053, OT/12/059) and the European Research Council (ERC, Starting Grant LIGHT 307523).

Notes and references

1 A. Dhakshinamoorthy, M. Opanasenko, J. Čejka and H. Garcia, *Catal. Sci. Technol.*, 2013, **3**, 2509–2540.

2 J. Lee, O. K. Farha, J. Roberts, K. A. Scheidt, S. T. Nguyen and J. T. Hupp, *Chem. Soc. Rev.*, 2009, **38**, 1450–1459.

3 P. García-García, M. Müller and A. Corma, *Chem. Sci.*, 2014, **5**, 2979–3007.

4 M. Savonnet, S. Aguado, U. Ravon, D. Bazer-Bachi, V. Lecocq, N. Bats, C. Pinel and D. Farrusseng, *Green Chem.*, 2009, **11**, 1729–1732.

5 J. Juan-Alcañiz, E. V Ramos-Fernandez, U. Lafont, J. Gascon and F. Kapteijn, *J. Catal.*, 2010, **269**, 229–241.

6 K. S. Park, Z. Ni, A. P. Côté, J. Y. Choi, R. Huang, F. J. Uribe-Romo, H. K. Chae, M. O'Keeffe and O. M. Yaghi, *Proc. Natl. Acad. Sci. U. S. A.*, 2006, **103**, 10186–10191.

7 C. Chizallet, S. Lazare, D. Bazer-Bachi, F. Bonnier, V. Lecocq, E. Soyer, A. A. Quoineaud and N. Bats, *J. Am. Chem. Soc.*, 2010, **132**, 12365–12377.

8 L. H. Wee, T. Lescouet, J. Ethiraj, F. Bonino, R. Vidruk, E. Garrier, D. Packet, S. Bordiga, D. Farrusseng, M. Herskowitz and J. A. Martens, *ChemCatChem*, 2013, **5**, 3562–3566.

9 B. Murillo, B. Zornoza, O. de la Iglesia, C. Téllez and J. Coronas, *J. Catal.*, 2016, **334**, 60–67.

10 X. Zhou, H. P. Zhang, G. Y. Wang, Z. G. Yao, Y. R. Tang and S. S. Zheng, *J. Mol. Catal. A Chem.*, 2013, **366**, 43–47.

11 L. T. L. Nguyen, K. K. A. Le and N. T. S. Phan, *Chinese J. Catal.*, 2012, **33**, 688–696.

12 U. P. N. Tran, K. K. A. Le and N. T. S. Phan, *ACS Catal.*, 2011, **1**, 120–127.

13 K. L. Liu, A. V. Kubarev, J. Van Loon, H. Uji-I, D. E. De Vos, J. Hofkens and M. B. J. Roeffaers, *ACS Nano*, 2014, **8**, 12650–12659.

14 A. V. Kubarev, K. P. F. Janssen and M. B. J. Roeffaers, *ChemCatChem*, 2015, **7**, 3646–3650.

15 Z. Ristanović, J. P. Hofmann, G. De Cremer, A. V. Kubarev, M. Rohnke, F. Meirer, J. Hofkens, M. B. J. Roeffaers and B. M. Weckhuysen, *J. Am. Chem. Soc.*, 2015, **137**, 6559–6568.

16 Z. Ristanović, A. V. Kubarev, J. Hofkens, M. B. J. Roeffaers and B. M. Weckhuysen, *J. Am. Chem. Soc.*, 2016, **138**, 13586–13596.

17 M. B. J. Roeffaers, G. De Cremer, H. Uji-i, B. Muls, B. F. Sels, P. A. Jacobs, F. C. De Schryver, D. E. De Vos and J. Hofkens, *Proc. Natl. Acad. Sci. U.S.A.*, 2007, **104**, 12603–12609.

18 E. Stavitski, M. H. F. Kox and B. M. Weckhuysen, *Chem. - A Eur. J.*, 2007, **13**, 7057–7065.

19 Z. Ristanović, M. M. Kerssens, A. V. Kubarev, F. C. Hendriks, P. Dedecker, J. Hofkens, M. B. J. Roeffaers and B. M. Weckhuysen, *Angew. Chemie - Int. Ed.*, 2015, **54**, 1836–1840.

20 M. B. J. Roeffaers, B. F. Sels, H. Uji-I, F. C. De Schryver, P. A. Jacobs, D. E. De Vos and J. Hofkens, *Nature*, 2006, **439**, 572–575.

21 X. Zhou, N. M. Andoy, G. Liu, E. Choudhary, K.-S. Han, H. Shen and P. Chen, *Nat. Nanotechnol.*, 2012, **7**, 237–41.

22 X. Zhou, W. Xu, G. Liu, D. Panda and P. Chen, *J. Am. Chem. Soc.*, 2010, **132**, 138–146.

23 P. Valvekens, D. Jonckheere, T. De Baerdemaeker, A. V. Kubarev, M. Vandichel, K. Hemelsoet, M. Waroquier, V. Van Speybroeck, E. Smolders, D. Depla, M. B. J. Roeffaers and D. De Vos, *Chem. Sci.*, 2014, **5**, 4517–4524.

24 M. B. J. Roeffaers, G. De Cremer, J. Libeert, R. Ameloot, P. Dedecker, A. J. Bons, M. Buckins, J. A. Martens, B. F. Sels, D. E. De Vos and J. Hofkens, *Angew. Chemie - Int. Ed.*, 2009, **48**, 9285–9289.

25 H. Bux, F. Liang, Y. Li, J. Cravillon, M. Wiebcke and J. J. Caro, *J. Am. Chem. Soc.*, 2009, **131**, 16000–16001.

26 D. B. Murphy and M. W. Davidson, *Fundamentals of Light Microscopy and Electronic Imaging: Second Edition*, John Wiley & Sons, Inc., Hoboken, NJ, USA, 2012.

27 C. Chizallet and N. Bats, *J. Phys. Chem. Lett.*, 2010, **1**, 349–353.

28 J. Canivet, M. Vandichel and D. Farrusseng, *Dalt. Trans.*, 2016, **45**, 4090–4099.

29 P. Valvekens, F. Vermoortele and D. De Vos, *Catal. Sci. Technol.*, 2013, **3**, 1435–1445.

30 P. Dedecker, S. Duwé, R. K. Neely and J. Zhang, *J. Biomed. Opt.*, 2012, **17**, 126008.